# Fuse Modeling for Reliability Study of Power Electronic Circuits

Bahman, Amir Sajjad; Iannuzzo, Francesco; Blaabjerg, Frede

*Published in:*
Proceedings of the 2017 IEEE Applied Power Electronics Conference and Exposition (APEC)

*DOI (link to publication from Publisher):*
10.1109/APEC.2017.7930792

*Publication date:*
2017

*Document Version*
Accepted author manuscript, peer reviewed version

# Fuse Modeling for Reliability Study of Power Electronic Circuits

Amir Sajjad Bahman, Francesco Iannuzzo, Frede Blaabjerg
Center of Reliable Power Electronics (CORPE)
Department of Energy Technology, Aalborg University, 9220 Aalborg, Denmark
asb@et.aau.dk, fia@et.aau.dk, fbl@et.aau.dk

***Abstract*—This paper describes a comprehensive modeling approach on reliability of fuses used in power electronic circuits. When fuses are subjected to current pulses, cyclic temperature stress is introduced to the fuse element and will wear out the component. Furthermore, the fuse may be used in a large variation of ambient temperature, e.g. in deserts and the accumulated damage in the fuse elements is gradually increasing due to thermo-mechanical stress that results in resistance increase and further unexpected failures. Consequently, the electrical characteristics of the fuse like $I^2t$, breaking capacity, and rated voltage/current are opposed to shift in time to effect early breaking during the normal operation of the circuit. Therefore, in such cases, a reliable protection required for the other circuit components will not be achieved. The thermo-mechanical models, fatigue analysis and thermo-electrical models of fuses are presented by FEM simulations in order to identify the important factors affecting the performance of fuses at different ambient temperatures and cycling operation.**

***Keywords—fatigue; finite element method; fuse; thermal stress; reliability.***

## I. INTRODUCTION

Although industries demand for new power electronic technologies, their product reliability depends on protecting their power circuits from overcurrent and short-circuit events [1]. For this reason, current-limiting fuses are widely used for protection of power electronic circuits against short-circuits and using the fuses is inevitable in different industries [2]. This could for instance be a transfer molded integrated power module which in case of short-circuit could explode and endanger the user by loss of the necessary dielectric blocking capabilities. However, the reliability of fuses has not been sufficiently investigated so far.

The most common fuse is the cartridge type. It consists of a tube – usually ceramic – containing one or more fuse elements which are soldered at each end to metal caps fitted over the ends of the tube. The key part of a fuse is the fuse element that is made of a high conductive material – usually a pure silver strip – and is shaped with a number of regions of reduced cross-sectional area commonly referred to as 'necks' or 'notches' (Fig. 1). They are mainly these regions that determine the operating characteristics of the fuse [3]. As the current flows through the fuse element some heat is generated due to its internal resistance. The heat power generated in the fuse element is proportional to the square of the current through it. When the current is lower than the fuse current rating, the heat is dissipated in the fuse body in stationary regime. Increasing the current beyond the nominal levels causes to higher power that fuse can dissipate, leading to cataclysmic thermal runaway. The center of the fuse element rapidly gets to the melting point. As the resistance of the molten metal is higher than the solid, more heat is generated in the fuse element that, in turn, intensifies the melting process and leads to the breakage of the current pathway. Usually the breakage of the fuse element is followed by an arcing phase that will remain until the current zeroes.

The fuse element is surrounded with an arc quenching material – usually sand – which extinguishes the arc when the element melts [4]. It is worth to point out that of course fuses are not supposed to open for other reasons than the expected one, i.e. circuit protection. By a proper selection and derating power cycles, fuses will not have problems at typical ambient temperatures. This means to do the reliability tests – e.g. active power cycling – prior to installation of fuse in the circuit that model the real-field mission profiles [5]-[7]. However, in harsh environments, temperature cycling may cause unexpected failures [8]. Unfortunately, the number of thermal cycles a fuse can withstand is not a design parameter for the manufacturer and the typical climatic tests last only 5-10 cycles, which is way lesser than real operating conditions. Therefore, there is still little knowledge on which parameters in the fuse are the relevant factors on the thermal cycling behavior. This paper proposes fuse models to be used in reliability analysis for real-field mission profiles. The models can also be used to manufacture fuses that withstand a longer lifetime with the same electrical specifications. In section II the fuse structure, material properties and the thermal stress analysis will be discussed. Section III is dedicated to the structural analysis of the fuse with transient cycling operation.

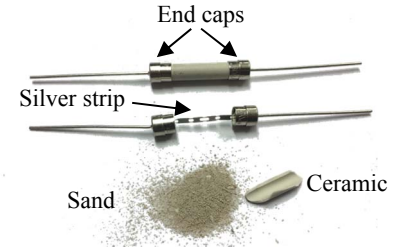


Fig. 1. Cartridge fuse and fuse element.

In section IV sensitivity of the stress on the fuse element by variation of some operational and geometrical factors will be presented. Based on the given discussions, a fatigue analysis will be presented in section V based on a specified temperature profile. Section VI is devoted to the electrical modeling of the fuse considering the variation of ambient temperature. Finally, the conclusions and some suggestions to use the fuse modeling in reliability analysis of power electronics will be presented.

## II. Thermal Stress Analysis of Fuses

In order to analyze the behavior of the fuse in thermal cycling, the fuse element is modeled in ANSYS Mechanical APDL 16.2 [9]. The following analysis is limited to a thermo-mechanical analysis of the silver strip. Thus the ceramic tube and, end-caps and wires will not be considered. However, their influence on the silver strip is included as the heat-flux, mechanical support and displacement. The silver strip is made of silver 99% pure and is encapsulated in the ceramic tube filled with sand (see Fig. 1). The silver strip is soldered to the copper end-caps with a solder material - typically a solder alloy of composition: $Zn_{85}Al_{15}$ or commercially pure zinc $Zn_{100}$. All materials are assumed to be homogeneous and isotropic. Material properties of interest are given below:

**Silver strip: Commercially pure Silver [10]:**

- Density = 10.5E-6 kg/mm$^3$
- Modulus of elasticity = 82.7E3 N/mm$^2$
- Poisson's ratio = 0.37
- Yield Strength = 54 N/mm$^2$
- Ultimate tensile strength = 210 N/mm$^2$
- True fracture stress = 235 N/mm$^2$
- Percent elongation at fracture = 46%
- Thermal conductivity = 0.429 W/mm·K
- Specific heat = 235 J/kg$^\circ C$
- Thermal expansion coefficient = 19.5E-6
- Melting temperature = 962$^\circ C$

**Solder: Commercially pure Zinc [10]:**

- Density = 7.140E-6 kg/mm$^3$
- Modulus of elasticity = 104.5E3 N/mm$^2$
- Poisson's ratio = 0.25
- Thermal conductivity = 0.108 W/mm·K
- Specific heat = 395 J/kg$^\circ C$
- Thermal expansion coefficient = 23.0E-6
- Melting temperature = 419 $^\circ C$

Initially, only the thermal behavior is considered. Afterwards, effects of pre-tension, which is built up during manufacturing, are considered later on. During the lifetime of the fuse element, the entire structure is heated and cooled with thermal loads, as categorized in the following points:

- Typical accelerated thermal load: [25°C - 50°C], [25°C - 60°C], [25°C - 70°C], [25°C - 80°C].

The *typical* scenario is thermal loads that are actually experienced in service. In service the fuse structure experiences one thermal cycle a day. The design goal is to have an expected life time of 10 years (360 days), thus a total of 3600 cycles. The design load case is referred to as the "*Desert Scenario*", where thermal loads are in the *typical* category with the following distribution of temperature range cycles:

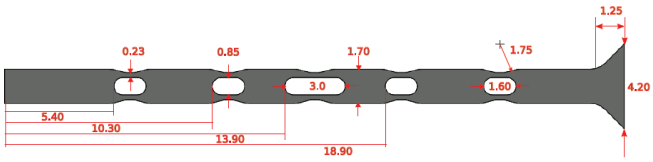


Fig. 2. CAD drawing of the silver strip with key dimensions.

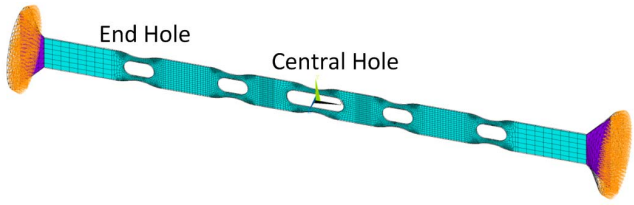


Fig. 3. Isometric view of the meshed geometry.

- 1200 cycles of $\Delta T$ = 55°C - [25°C - 80°C],
- 1500 cycles of $\Delta T$ = 45°C - [25°C - 70°C],
- 900 cycles of $\Delta T$ = 35°C - [25°C - 60°C].

Accelerated fatigue tests have been performed on the fuses, showing failure in the silver strip. Hence, in the following, the silver strip is of main interest. Specifically, the failure occurs in the groove/hole regions of the silver strip, hence away from the solder region and these are thus of less interest. The silver strip along with its key dimensions is shown in Fig. 2. Depending on the electric current experienced by the fuse, different versions of the fuse are available. In this paper, the 500V / 30A fuse is considered, having a silver strip thickness of 0.11 mm.

A thermal-stress analysis is performed using ANSYS. The final mesh is shown in Fig. 3. In service, the entire fuse element is heated and cooled in a given temperature range. Reconsidering the construction of the fuse and the material properties of the silver strip in comparison to the ceramic tube, it is a reasonable assumption, that only the ends of the silver strip (the solder volumes) are subjected to a prescribed temperature-profile. For example, the thermal conductivity of the ceramic tube is in the order of 1 W/m·K whereas silver has a thermal conductivity of 430 W/m·K - and similar difference in physics for the thermal coefficient of expansion and the specific heat. Based on this, boundary conditions as shown in Fig. 3, in which the orange triangles represent prescribed temperatures, are applied. As stated earlier, the silver strip is surrounded by sand. The thermal conductivity of the sand is relatively small compared to that of silver. However, the heat transfer to the surroundings is estimated using the following formula:

$$H/A = k\frac{\Delta T}{\Delta z} = -0.00595\ W/mm^2K \qquad (1)$$

The heat flow, $H$, per area $A$, is roughly estimated by assuming a constant temperature difference of $\Delta$T = 55°C, a constant thermal conductivity of sand k = 0.2E3 W/mm·K,

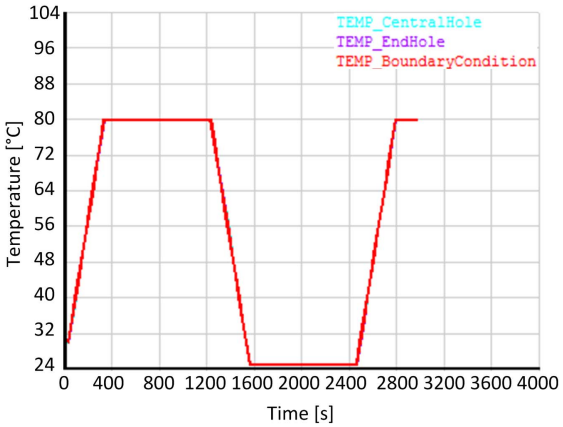


Fig. 4. Thermal load profile, along with thermal response at End Hole and Central Hole locations.

and $\Delta z$ = 1.85 mm, being the distance from the silver strip to the ceramic tube. The heat flux is negative, since heat is transferred from the silver strip to the surroundings.

The thermal loading curve is shown as the blue curve *Boundary Condition* in Fig. 4. Here, the temperature range is $\Delta T$ = 55˚ [25˚C - 80˚C], the rise time $t_{rise}$ = 10˚C/*min*, and the hold time $t_{hold}$ = 15min = 900s. Apart from showing the prescribed temperature at the model boundary, the figure also shows the thermal response at the End Hole and the Central Hole locations. Note there is no noticeable difference in temperature at a given time as the temperature is applied sufficiently slowly such that a uniform temperature exists throughout the silver strip. The current thermal profile is more representative for an in-service cycle which lasts for an entire day, and thus a uniform temperature throughout the silver strip should be expected in service at any time.

## III. Structural Stress Analysis of Fuses

In the subsequent structural analysis, the silver strip is considered to be clamped, that is X-,Y-, and Z-components of displacement are prescribed as zero. The thermal coefficient of expansion of the silver strip is in the order of 10-50 times the thermal coefficient of expansion of the ceramic tube. Based on this, it is assumed that the ceramic tube doesn't expand or contract during thermal cycling. Nevertheless, from the silver strip point of view, this assumption is conservative, since it is more restrained if the ceramic tube is allowed to expand/contract with the silver strip. Given the uncertainties in both the material data, fatigue data and other assumptions, some conservatism is acceptable. Structural analysis is implemented by considering both elasticity and plasticity in the material model. This is done based on the true stress-strain curve in [10]. Rate-independent plastic behavior for the silver strip is described using a multilinear kinematic hardening law, which has the benefit of modeling the Bauschinger effect, at least to some extent, as opposed to the isotropic hardening model. Whenever cyclic loading is to be modeled, the kinematic hardening model is preferred over the isotropic hardening model.

Considering next the thermal stresses, a contour plot of the equivalent Von Mises Stress reveals that there is a stress

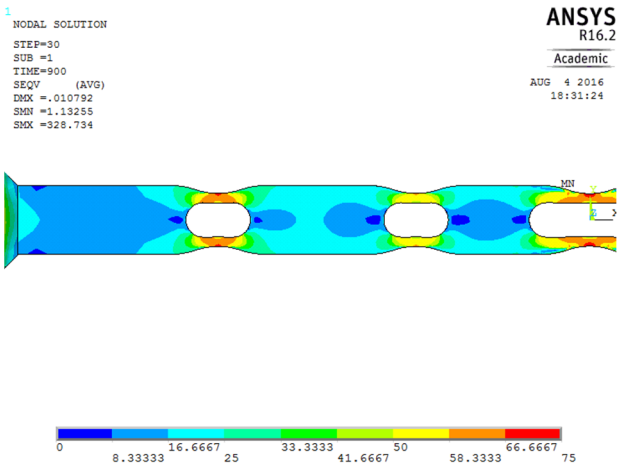


(a)

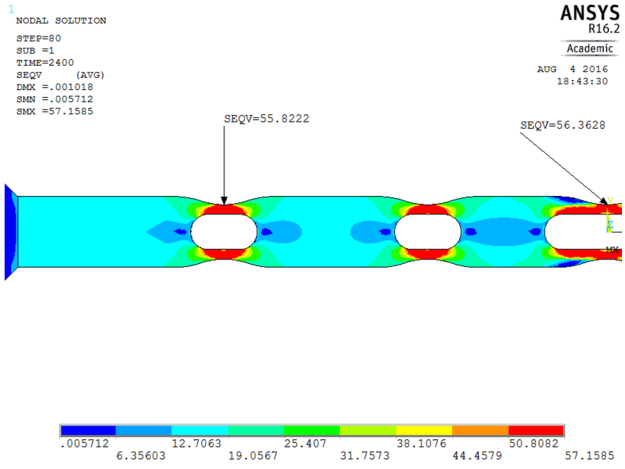


(b)

Fig. 5. Thermal range $\Delta T$ = 55˚C [25˚C - 80˚C]: (a) Von Mises stress at TIME = 900s, (b) Von Mises stress at TIME = 2400s.

concentration at the groove/notch root. Contour plots of Von Mises stress at TIME = 900s and TIME = 2400s are shown in Fig. 5.a and Fig. 5.b respectively for the temperature range $\Delta T$ = 55˚C [25˚C - 80˚C]. Stresses at the notch root of the End Hole and Central Hole are pointed out. These points are identified as regions of locally high stresses, and suggest the amount and location of local plasticity. At TIME = 900s there is a maximum stress of 73 MPa and 69 MPa at the notch root of the Central Hole and End Hole respectively. Thus slightly higher stresses are experienced at the Central Hole, which has been observed for every temperature range. The stress evolution over time at these locations is shown in Fig. 6.a. Only the X-component of stress is shown, since this is more informative than the Von Mises stress as it takes sign into consideration. Fig. 6.b shows the X-component of elastic (EPELX) and plastic (PPELX) strain in the notch root of the central hole. It is evident that large plastic strains occur, additionally, these are always compressive, whereas the elastic strain attains both positive and negative values. The net strain X-component is given as the sum of the elastic part and the plastic part. These are of interest when evaluating the fatigue

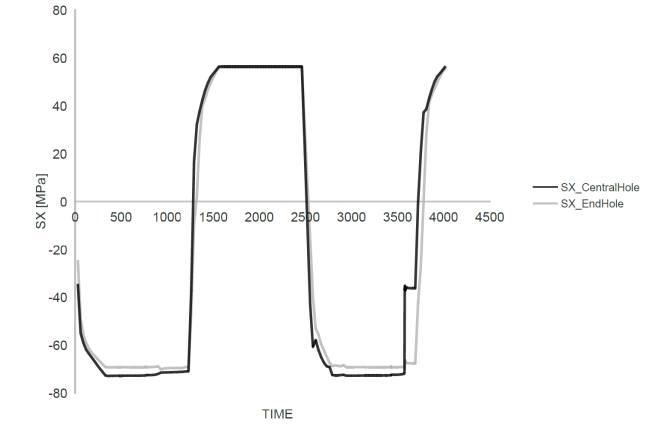


(a)

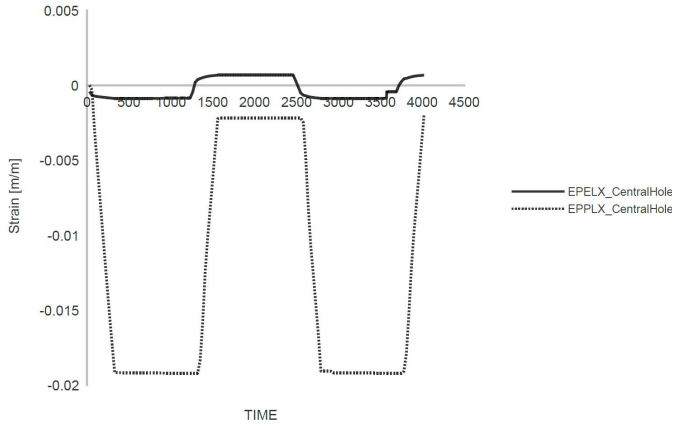


(b)

Fig. 6. (a) X-Component of stress over time at the notch root of Central Hole and End Hole; (b) Elastic and plastic X-strain components at Central Hole notch root.

strength according to a strain life approach. Due to the large amount of plastic deformation upon heating to 80˚C, large tensile stresses of around 56 MPa are developed when the specimen is cooled to the ambient temperature of 25˚C, which initially was a stress/strain free state.

Reconsidering the stress-time history, values for the stress range, minimum stress and maximum stress is given as: ΔSX = 129 MPa, $SX_{min}$ = -73 MPa, and thus $SX_{max}$ = 56 MPa. From here it is seen that there is a mean stress of: $SX_{mean}$ = - 8.5 MPa during a load cycle. It is noted that the mean stress is compressive, which is beneficial from a fatigue point of view, since only tensile stress is related to crack opening/growth.

## IV. Sensitivity Analysis of Fuses

### A. Sensitivity to temperature range

The results above concern the thermal load [80-25] ˚C having a $\Delta T$ = 55˚C. Similar analyses are performed for other thermal loads, as presented below:

- $\Delta T$ = 25˚C, for range [50-25] ˚C

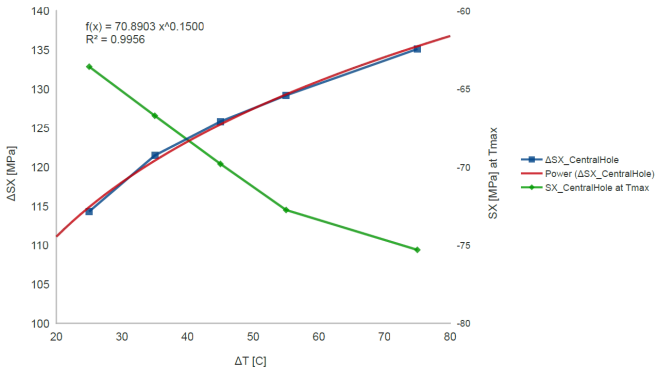


Fig. 7. Primary Y-axis: Temperature range ΔT versus absolute value stress range ΔSX. Secondary Y-axis: Temperature range ΔT versus SX. The stresses are measured at the notch root of the Central Hole. The reference temperature for zero strain is TREF=25˚C.

- $\Delta T$ = 35˚C, for range [60-25] ˚C
- $\Delta T$ = 45˚C, for range [70-25] ˚C
- $\Delta T$ = 55˚C, for range [80-25] ˚C
- $\Delta T$ = 75˚C, for range [90-15] ˚C

In this paper, the discussion is limited to a comparison between $\Delta T$ and the largest X-component of stress. By largest X-component of stress, is meant the largest absolute value of the stress X-component. This is seen to occur at times whenever the temperature is highest (e.g. TIME = 600s in Fig. 6.a). The location of the largest stress X-component is the notch root of the Central Hole. Results are shown in Fig. 7; here the stress range ΔSX versus ΔT are plotted along the primary Y-axis, and the values of SX versus ΔT are plotted along the secondary Y-axis. The values of ΔSX and SX are taken during the first cycle of loading. A power regression is performed on the (ΔSX - ΔT) data, resulting in the curve *f*. It is noticed that there is a good correlation with the power regression ($R^2$ = 0.9956), and it seems fair to interpolate values of (ΔSX - ΔT) with the above equation. The data for (SX - ΔT) is, however, not as smooth but the tendency is the same; the absolute value of the slope decreases with increasing ΔT.

### B. Sensitivity to geometry

The main focus of this sensitivity analysis is to check the model sensitivity to small changes in geometry in regions of high stresses. As the main function of the fuse is to break the current by melting the fuse element, there is not much degree of freedom to change the geometry, especially in the thickness and the length of the fuse element as are important factors in the fuse electrical specifications. So the focus is on the notched regions. The following sensitivity studies are considered:

- Effects of changing notch radii
- Effects of changing notch depth

Starting out by considering the effect of changing the notch radii. The measurements from Fig. 2 are fixed, except the notch radii of 1.75 mm which is determined from visual

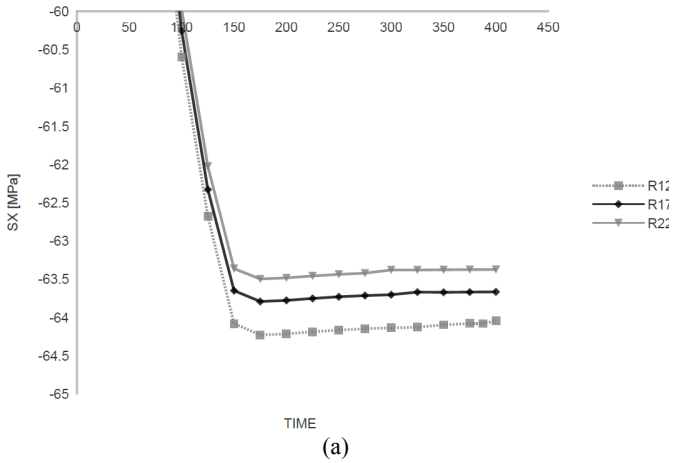


(a)

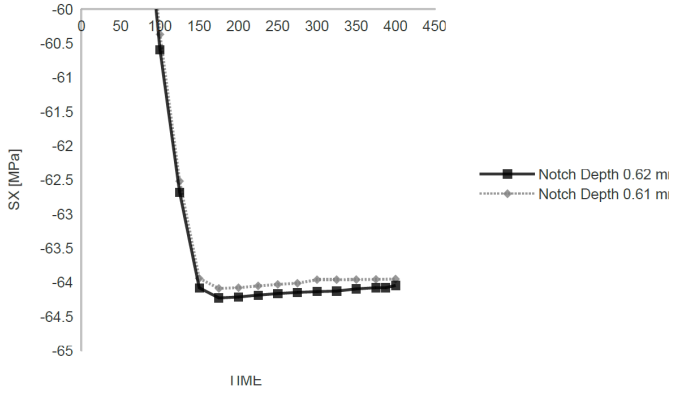


(b)

Fig. 8. (a) X-Component of stress over time at the notch root of Central Hole for different notch radii. (b) X-Component of stress over time at the notch root of Central Hole for various notch depths.

inspection. Additional points of critical stress are identified at the notch root, thus the notch radii. Thermal stress analyses are performed with notch radii of $R$ = 1.75 mm ± 0.50 mm. For these analyses, the specimen is heated from 25˚C to 50˚C with a rise time of $t_{rise}$ = 10˚$C/min$ and then kept at 50˚C for around 4 min.

The X-component of stress versus the time is plotted in Fig. 8.a for different notch radii. It is seen from the graph that changing the notch radii 0.50 mm has little/negligible influence on the stress results ±0.50 MPa. It is obvious, that increasing the notch radius reduces the stress concentration and hence the stress. Nevertheless, the influence on the stress magnitude is small, and according to the model, there is no need to obtain more accurate measurements of the notch radii.

Secondly, the effect of decreasing the notch depth by 10 µm is examined. According to Fig. 2 the notch depth, $d_n$, is given as 0.195 mm. These +10 µm could for instance represent manufacturing tolerances. The effect on the stress at the notch root of the Central Hole is shown in Fig. 8.b. Again,

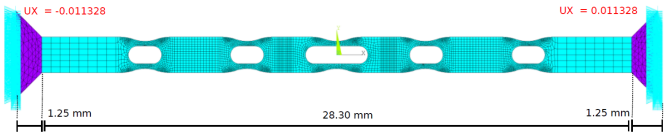


Fig. 9. Changing boundary conditions to represent pretensioning.

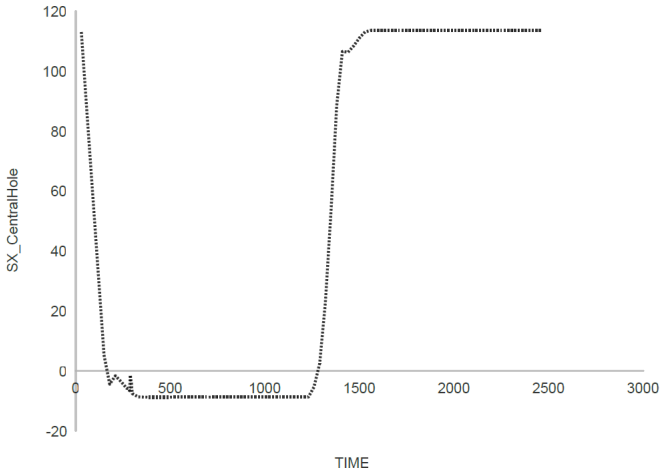


(b)

Fig. 10. (a) Stress-time history with thermal loading of [80-25] ◦C in existence of pre-tensioning. The X-component of stress at the Central Hole.

the effect of small geometric changes is small - around 0.5 MPa, and is not considered any further.

### C. *Sensitivity to pre-tensioning*

It is believed that pre-tensioning of the silver strip builds up during the manufacturing of the fuse. This occurs when the silver strip is soldered to the end-caps. The subsequent cooling of the solder material from its melting point $T_m$ = 419˚C to the room temperature $T$ = 25˚C, causes a contraction of the solder material and hence tension in the silver strip. In this section, a rough estimate of the effect of pre-tensioning is given. It is assumed that only the specimen is cooled from $T_m$ = 419˚C to $T$ = 25˚C. Thus the thermal contraction upon cooling is:

$$\delta = \alpha \Delta T L = 19.5E-6 \cdot 394℃ \cdot 30.8\,mm \approx 0.237\,mm \quad (2)$$

This is implemented as prescribed displacements in the X-direction at every end of the FE-model, as illustrated in Fig. 9. The effect on the stress-time history is shown in Fig. 10. At first, notice that at TIME = 0s tensile stress of around 112 MPa exists, thus tensile plastic deformation occurs due to the pre-tensioning alone. The response to the cyclic thermal loading, gives $SX_{max}$ = 112 MPa, $SX_{min}$ = -8 MPa hence a tensile mean stress of 60 MPa. The pre-tensioning shifts the stress-time curve upwards. That is, an increase in tensile stresses occurs, but a decrease in compressive stresses. From a fatigue point of view, it is important to notice that the mean

stress is shifted from being a beneficial compressive mean stress to become a detrimental tensile one.

## V. Fatigue Analysis

### A. Estimation of fatigue data

Ideally, fatigue data are obtained by testing the actual design under real load, temperature, and environmental conditions. The next best information comes from fatigue tests of specimens taken from the particular material as it is manufactured for the specimen. Failing to obtain this data, published fatigue data available in the literature or from the material manufacturers should be used, however, keeping in mind that these data will be for small, polished specimens tested in controlled environments. In absence of even these data, it will be necessary to make some estimation of the fatigue strength of the material based on data available from monotonic tests. Unfortunately, the last approach is what is used in this paper, since no fatigue data of better quality has been available.

Any thermal/mechanical loads that vary with time can potentially cause fatigue. The loads behavior may vary significantly from one application to another. However, the shape of the load-time waveform seems not to have any significant effect on fatigue failure (in absence of corrosion) [11]. Hence, the current saw-tooth like representation of the thermal load is acceptable. Also, the presence or absence of periods of rest in the load history is not significant (as long as the environment is non-corrosive). This is also seen in the FE simulations; no further change in stress/strain happens when the thermal load reaches for instance the maximum temperature - from this point the stress curve is horizontal as shown in Fig. 6 (at least for reasonable rise times). The significant factors are the amplitude and mean value of the stress/strain – time waveform and the total number of stress/strain cycles.

Since the loading is thermal, one should be aware of high-temperature effects, such as creep/relaxation and various metallurgical properties. However, high temperature effect is effective in the ranges above 30% to 40% of the melting point of the material. Recalling that the melting temperature of the pure silver is 962°C, 30% of this is approximately 289°C, while the thermal loads don't exceed 90°C. Thus high temperature effects can be neglected.

Recalling the design load case: *Desert Scenario*, where thermal loads are with the following distribution of temperature range cycles:

- 1200 cycles of $\Delta T$ = 55°C – [80-25] °C
- 1500 cycles of $\Delta T$ = 45°C – [70-25] °C
- 900 cycles of $\Delta T$ = 35°C – [60-25] °C

This gives a total of $N_f$ = 3.6E3 cycles to failure. Based on the number of stress/strain cycles the specimen is expected to undergo in its lifetime, the fatigue is categorized as either low cycle fatigue (LCF) and high cycle fatigue (HCF) [11]. A common division line between the two regimes is N=10E3, however other suggests somewhere in between 10E2 and 10E4. Nevertheless, the main part of the specimen's life, when subjected to 3.6E3 cycles, is in the LCF regime. Three main methods for fatigue life-assessment are used in general: Stress-life approach (S-N), strain life approach ($\varepsilon$-N) and fracture mechanics approaches:

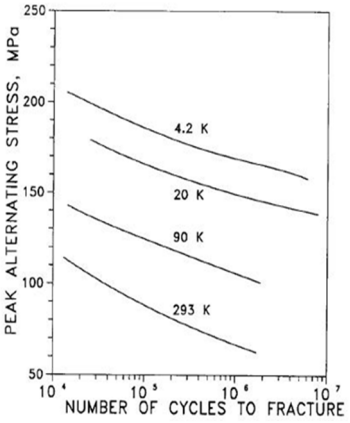


Fig. 11. S-N curves. Fully reversed loading. Stress amplitude as function of number of cycles to failure. Axial testing [10].

- (S-N)-approach: This method is mainly used in the HCF regime and for infinite life design. It is mainly suited for applications, in which, stresses and strains in all regions of the specimen remain in the elastic region, so no local yielding occurs to initiate a crack. It is an imprecise method in terms of defining the true local stress/strain state in the specimen, especially for LCF with yielding [11].
- ($\varepsilon$-N)-approach: When yielding occurs, strain is a better measure for material behavior than stress. The method is most often applied to LCF and finite life design where cyclic stresses are high enough to cause local yielding [11].

Both approaches are applicable for life assessment of the silver strip. However, the preferred choice is the ($\varepsilon$-N)-approach due to the local plasticity experienced in the notched regions and regions around the holes. From the literature [10] S-N curves in the HCF regime is available as shown in Fig. 11. However, no data is available in the LCF regime, which is of interest. Additionally, the data is obtained for polished, un-notched specimens tested in controlled environments; hence the need for correction factors according to [11] is evoked. Additionally, the fatigue data is obtained under axial testing, which is relevant when determining correction factors. Nevertheless, the data can be used as a help to estimate the fatigue properties in the LCF regime.

Strain-life ($\varepsilon$-N) – curves are approximated based on monotonic material properties. Two approaches are used:

- The Method of Universal Slopes
- Four-Point Method

The above approaches are described in [12] and [13]. In short, the strain is decomposed into an elastic part and a plastic part. Elastic strain - life curves and plastic strain - life

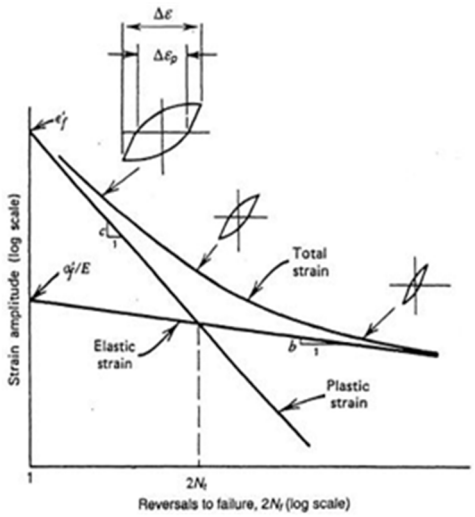


Fig. 12. Illustration of the basic steps in estimating strain-life curves. [12].

curves are then estimated as straight lines in log-log coordinate systems, as illustrated in Fig. 12.

It is worth to note that, at short lifetimes, the plastic line is dominating, while at high lifetimes the elastic line is the dominating one. The transition fatigue life, $N_t$, is the life at which the elastic and plastic lines intersect. At cycles lower than $N_t$, the deformation is mainly plastic, and at cycles higher than $N_t$ the deformation is mainly elastic. The transition fatigue life can be just a few cycles for high-strength metals and on the order of $10^5$ cycles for metals with ductile behavior [12]. Thus even at relatively long life, significant plastic strain can be present. Considering the low yield strength of 54 MPa of silver and the S-N curve for smooth specimens as given by [10] in Fig. 11, and the fact that silver is relatively ductile, a rather high transition fatigue life can be expected. Fig. 13 shows three strain-life curves. One based on the method of universal slopes, and two based on the Four-Point Method. The *Corrected Four-Point Method* has shifted the transition life from $N_t \approx 6 \cdot 10^4$ towards higher cycles ($N_t \approx 1 \cdot 10^5$) based on the above discussion. This results in higher lifetimes in the life-range of interest. The method of universal slopes assumes a constant slope of the elastic and plastic lines for every metal. The slopes are determined by curve fitting to experimental data performed on 47 metals including steels, aluminum and titanium. The Four-Point method allows different slopes based on monotonic properties and is in this sense more flexible than the method of universal slopes.

### *B. Palmgren-Miner Linear Damage Rule*

During its life time, the fuse is subjected to loads of varying amplitude/range. Whether failure has occurred or not can be evaluated by the linear damage rule proposed by Palmgren and Miner, information of which can be found in [13]. The rule defines a damage D which should be less than unity for no failure:

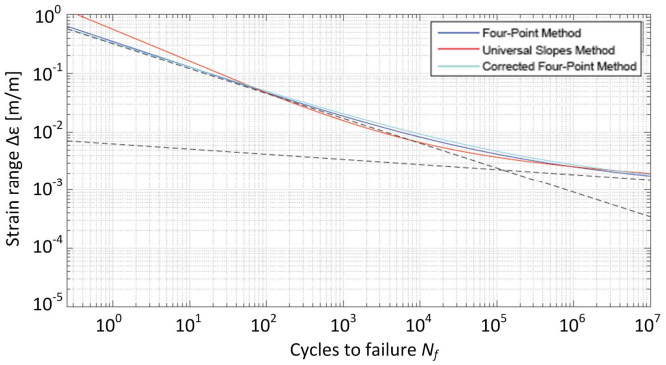


Fig. 13. Estimate of (ε-N) - curves. Fully reversed loading. Strain range Δε as function of number of cycles to failure.

$$D = \sum_{i=1}^{n} \frac{n_i}{N_{fi}} = 1 \tag{3}$$

Where $n_i$ is the number of cycles experienced by the specimen for the i-th load, and $N_{f\,i}$ is the number of cycles to failure if only the i-th load were acting. The damage rule can be applied to both strain-life and stress-life approaches. According to the design load case *desert scenario*, the following values of $n_i$ are given:

$n_1$=1200 for $\Delta T$ = 55˚C - [25˚C- 80˚C]

$n_2$=1500 for $\Delta T$ = 45˚C - [25˚C - 70˚C]

$n_3$=900 for $\Delta T$ = 35˚C - [25˚C - 60 ˚C]

and by using the corrected Four-Point Method the $N_{f\,i}$ values are given:

$$N_{f1}^{\Delta T55} = 1300$$

$$N_{f2}^{\Delta T45} = 2900$$

$$N_{f3}^{\Delta T35} = 7900$$

So, the damage D predicted from the corrected Four Point method will be 1.55 that predicts fatigue failure with the given profile.

## VI. Electrical Model of the Fuse

The main electrical parameters to be considered in the fuse selection are $I^2t$, breaking capacity, and rated voltage and rated current. However, the breaking capacity tests of fuses are done performed at 25°C and will be affected by the change of ambient temperature. One of the targets in the reliability analysis of the fuses is to define the temperature dependent behavior of the fuse during the life cycles and derating caused by thermal stresses on the fuse. In a fuse element, the highest current density is around the holes (Fig. 14), so the shape of these holes is critical to define the current carrying capacity of the fuse. Moreover, different temperature ranges cause to re-rating of the fuse and the current carrying capacity of the fuse will be more affected with higher thermal stresses. For example, as it is observed in Fig. 15, with higher thermal stress ranges, the fuse rating is decreased significantly.

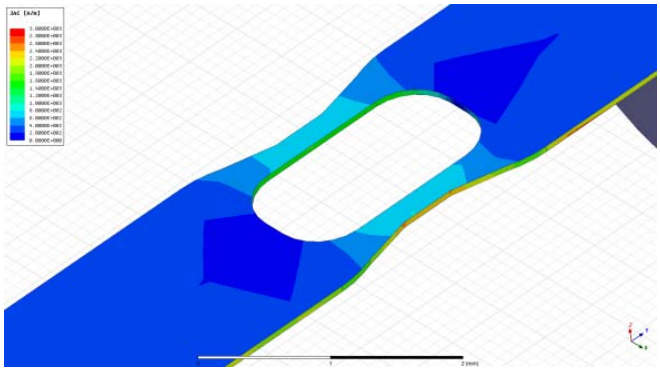

Fig. 14. Current distribution around the hole.

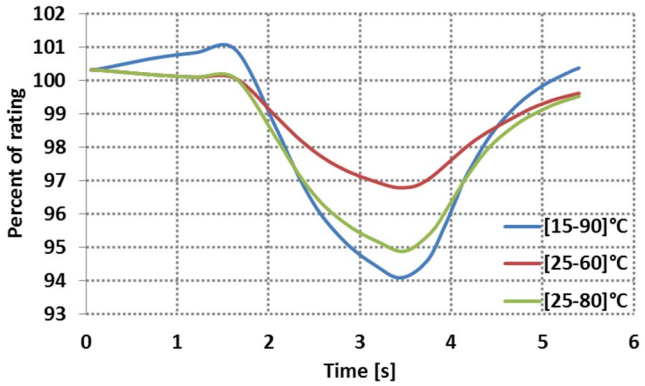


Fig. 15. Temperature cycling effects on current carrying capacity of the fuse.

## VII. Conclusions

In this paper, a comprehensive study has been devoted to reliability analysis of cartridge fuses for the first time by variation of ambient temperatures. In contrast to existing reliability tests that are implemented on fuses in different current/voltage ranges, the climatic tests on a typical fuse is only done 5-10 cycles according to standards that are far from the real cases. This may cause to wrong assessment of fuses and the failure mechanism in the device will be unknown. So, the paper focuses on comprehensive thermo-mechanical analysis of the fuses in different temperature ranges to investigate the effect of thermal cycling on the behavior of fuses. The FEM structural analysis proves that the notches regions experience higher stress in a single thermal cycling. A fatigue analysis has been performed for longer term cyclic operation that predicts failure with a given desert temperature profile. Finally, the effect of ambient temperature variation on the re-rating of the fuse analyzed. The proposed fuse models can be used in a mission-profile based approach that considers the reliability in the design and application of fuses. Moreover, the proposed models can be used to improve the thermal cycling capability of fuses and to increase the lifetime in real operating conditions.

## Acknowledgment

The authors express their special thanks to Grundfos Holding A/S for providing the fuse samples and field data that have been used for the purpose.

## References

[1] D. J. A. Wiliams, “Fuses and Protective relays,” *Electrical Power Engineer’s Handbook,* Elsevier, pp. 219-245, 2005.

[2] Fuse Characteristics, Terms and Consideration Factors, Littlefuse, 2009.

[3] J. D. Twibell, C. C. Christie, “The Forensic Examination of fuses,” Science and Justice, vol. 35, no. 2, pp. 141-149, 1995.

[4] R. Wilkins, H. Cynthia Cline, “An Advanced Applications Tool to Enhance theFuse Protection of Power Semiconductors,” in *Proc. Industry Applications Society Annual Meeting*, pp. 1226-1230, 1993.

[5] A. S. Bahman, F. Iannuzzo, F. Blaabjerg, “Mission-profile-based stress analysis of bond-wires in SiC power modules”, *Microelectron. Reliab.*, Vol. 64, pp. 419-424, Sep. 2016.

[6] A. S. Bahman, K. Ma, P. Ghimire, F. Iannuzzo, and F. Blaabjerg, "A 3D lumped thermal network model for long-term load profiles analysis in high power IGBT modules," *IEEE J. Emerg. Sel. Topics Power Electron.*, vol. 4, no. 3, pp. 1050-1063, Sep. 2016.

[7] H. Wang, M. Liserre, F. Blaabjerg, P. de Place Rimmen, J. B. Jacobsen, T. Kvisgaard, and J. Landkildehus, “Transitioning to Physics-of-Failure as a Reliability Driver in Power Electronics,” *IEEE J. Emerg. Sel. Topics Power Electron.*, vol. 2, no. 1, pp. 97-114, March 2014.

[8] X. Z. Meng, J. G. J. Sloot, “Reliability Concept for Electric Fuses,” *IEE Proc. –Sci. Meas. Technol.*, vol. 144, no. 2, pp. 87-92, Mar. 1997.

[9] ANSYS® Academic Research, Release 16.2, *ANSYS Mechanical*.

[10] D. R. Smith, and F. R. Fickett, “Low-Temperature Properties of Silver,” *Journal of Research of the National Institute of Standards and Technology*, vol. 100, no. 2, pp. 119-171, Apr. 1995.

[11] Robert L. Norton, *Machine Design: An Integrated Approach*, 5th ed. Pearson 2014.

[12] U.U. Muralidharan, S.S. Manson, “A Modified Universal Slopes Equation for Estimation of Fatigue Characteristics of Metals.,” *ASME. J. Eng. Mater. Technol*, vol. 110, no. 1, pp. 55-58, 1988.

[13] R. I. Stephens, A. Fatemi, R. R. Stephens, H. O. Fuchs, *Metal Fatigue in Engineering*, 2. ed., Wiley 2001.